Materials Horizons

Accepted Manuscript

ROYAL SOCIETY OF CHEMISTRY

rsc.li/materials-horizons

Journal Name

RSCPublishing

COMMUNICATION

A significant cathodic shift in onset potential of photoelectrochemical water splitting for hematite nanostructures grown from Fe-Si alloys

Cite this: DOI: 10.1039/xoxxoooooox

Received ooth January 2013,
Accepted ooth January 2013

DOI: 10.1039/xoxxoooooox

www.rsc.org/

Lei Wang,[a] Chong-Yong Lee,[a] Robin Kirchgeorg,[a] Helga Hildebrand,[a] Julian Müller,[b] Erdmann Spiecker[b] and Patrik Schmuki [a,c,*]

Thermal oxidation of Fe to nanostructured hematite (wires, flakes) is currently widely investigated to produce efficient photoanodes for photoelectrochemical water splitting. The process carried on pure iron, however, has the key drawback that not only hematite but a layered structure of $Fe_2O_3/Fe_3O_4/FeO$ is formed where the thick suboxide layer underneath the Fe_2O_3 is highly detrimental for the photoresponse. In the present work, we show that suboxide formation can be largely suppressed if hematite nanowires/nanoflakes are thermally grown on Fe–Si alloys. For hematite structures grown on a Fe–Si alloy with 5 at.% Si, a photocurrent onset potential as low as 0.6 V_{RHE} can be reached (under AM 1.5 illumination and 1 M KOH). We believe that the results represent a key finding towards the formation of optimized hematite nanostructures using a thermal oxidation method.

Hematite (α-Fe_2O_3) has been considered as a promising anode material for photoelectrochemical (PEC) water splitting due to its narrow band gap energy (~2.2 eV), which is suitable for absorption of a large part (≈15%) of the solar spectrum.[1] Hematite has an indirect band gap with a comparably low optical absorption coefficient, and therefore an α-Fe_2O_3 photoanode should be considerably thick (typically, several 100 nm) to fully absorb incident light. However, the material has a poor conductivity and an extremely short hole diffusion length (~4 nm). To resolve this conflict between short hole diffusion length and low light absorption coefficient, frequently, vertically arranged one-dimensional (1-D) nanostructures such as tubes, wires or rods have been proposed.[2] In such photoanodes, the vertical direction serves as light absorption path while minority carriers can be transported orthogonally without much loss to the electrolyte.[3]

A most simple, cheap, and direct procedure to produce high aspect ratio nanostructures (e.g. 1-D α-Fe_2O_3 wires or others), is thermal oxidation of metallic iron. Under specific thermal annealing conditions, spontaneously, oxide whisker (or nanowire) growth can be observed.[4] Several reports on trials to optimize density and geometry of the grown Fe-oxide nanowires (NWs) or nanoflakes (NFs) exist.[4,5] Although these structures are very promising in morphology, the actual photocurrents obtained from such nanostructured electrodes are rather poor.[5a,6,7] This is to a large extent due to the formation of thick sub-oxide phases such as magnetite (Fe_3O_4) underneath the hematite structures. Under many thermal oxidation conditions, a $Fe_2O_3/Fe_3O_4/FeO$ gradient is formed. The thick Fe_3O_4/FeO suboxide layers are particularly detrimental to the photoresponse because these phases represent a barrier for charge transfer to the back contact.[4]

In the present paper, we report on an approach to largely suppress the formation of such thick suboxide scales. For this we use, instead of a pure Fe substrate, a Fe–Si alloy (with 5 at.% Si). We find that during the thermal oxidation process, Si is accumulated as a thin SiO_2 film at the metal/oxide interface – this provides a highly beneficial protection layer that prevents the growth of a several micrometer thick Fe_3O_4 layer underneath the α-Fe_2O_3 layer (SI, Figure S1). As a result, a considerable cathodic shift of the water-splitting onset potential to 0.6 V_{RHE} in 1 M KOH (under AM 1.5 100 mW cm^{-2}) for a hematite layer formed on a 5 at.% Si alloy can be observed.

Figure 1a and b show the top surface morphologies of Fe and Fe5Si substrates after the growth of oxide flakes by air annealing at 500 °C (insets) and after conversion to nanorods in Ar (600 °C). The conversion of flakes to rods is beneficial as it optimizes geometry and eliminates defects present in the NFs prepared in this method of oxidation.[1c,4b] In general, for the Si alloy a slightly lower density of

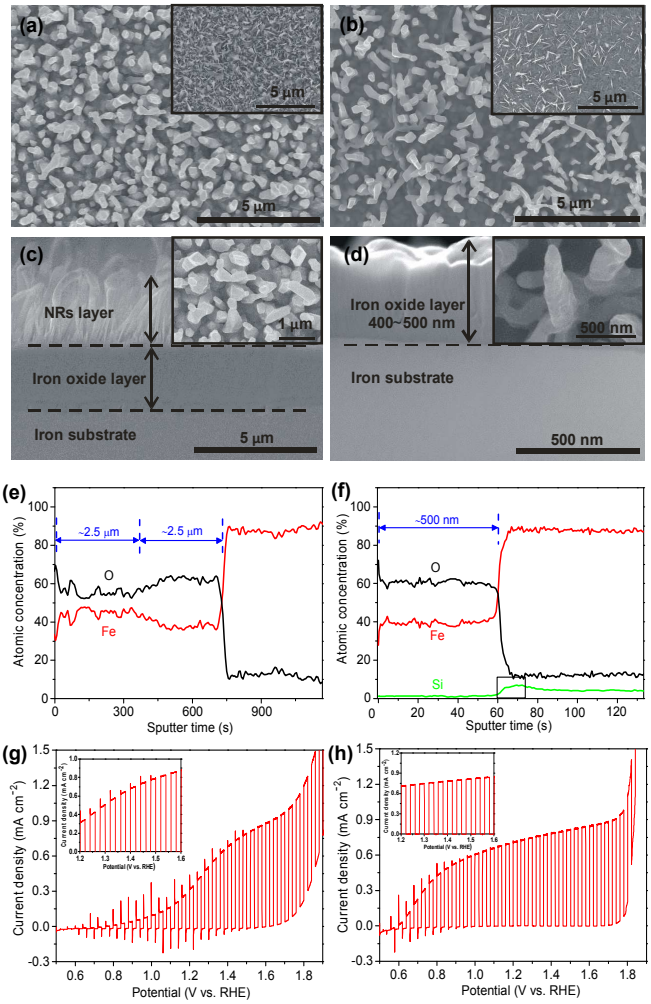

Figure 1. (a-d) SEM top views and cross-sections of oxide films resulting from (a,c) Fe and (b,d) Fe5Si alloy annealed at 500 °C for 0.5 h in air + 600 °C for 1 h in Ar. (Insets of a and b show the top views of samples annealed at 500 °C for 0.5 h in air; insets of c and d show the high magnification of top views of a and b); (e,f) corresponding element distribution of oxide layer of the corresponding annealed (e) Fe and (f) Fe5Si alloy; (g,h) current-potential characteristics with chopped light of the annealed (g) Fe and (h) Fe5Si alloy. Inset graphs show magnified views of the 1.2–1.8 V_{RHE} region for both spectra. Conditions: 1 M KOH solution (pH 13.6), 2 mV s^{-1} scan rate. Photocurrents are excited with AM 1.5, 100 mW cm^{-2} simulated sunlight.

NF and resulting nanorods formed on the substrate than on pure Fe (see Figures 1a-b and S2). After formation, NFs are in dense arrays with sharp apexes. The NFs are of ≈500 nm for short annealing times (SI, Figure S3), or up to approx. 1.5~2.5 μm long for longer time annealing (SI, Figure S2). The flakes have typically a width of 200~500 nm at the base that tapers down to approximately 10 nm at the tips. The resulting nanorods (after Ar annealing) typically have a length of ~2.5 μm and a diameter of 100~200 nm. A most significant difference between alloy and pure iron substrate is apparent from ion milled cross-section SEM images (Figure 1c and d) and Auger Electron Spectroscopy line scans (Figure 1e and f). The total

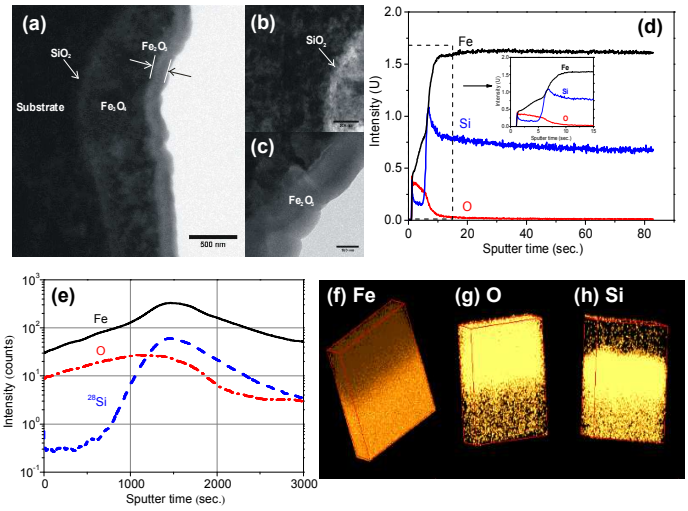

Figure 2. (a-c) TEM image of the annealed Fe5Si alloy; (d) GDOES elemental depth profiles of oxide layer of the Fe5Si alloy; (e) ToF-SIMS depth profile for Fe, O, and Si species of the annealed Fe5Si alloy; (f-h) ToF-SIMS-EDS mapping of Fe5Si alloy to show the distribution of Fe, O, and Si, respectively.

thickness of the composite oxide layer on the Fe substrate is with ~2.5 μm approximately five times thicker than on the Si containing alloy (~500 nm). (Please note that the top NR structure is not clearly visible in these cross sections due to the nature of the ion milling treatment. Please see SI, Figure S4.) The elemental profile (Figure 1f) shows that the FeSi alloy is strongly enriched in silicon at the metal/oxide interface. This is confirmed by GDOES (Figure 2d) and ToF-SIMS depth profiles (Figure 2e) where the elemental mapping (Figure 2h) shows a significantly higher intensity of the signal corresponding to Si at the metal/hematite interface. The finding is in line with general literature on the high temperature oxidation of Fe–Si alloys that show a reduced oxidation rate relative to pure iron.[8] Of then this is ascribed to Si effects on the grain growth mechanism of iron oxide films.

Figure 1g and h show the photoelectrochemical water splitting behavior under simulated sunlight AM 1.5 (100 mW cm^{-2}) conditions in 1 M KOH for pure Fe and the Fe5Si alloy. From the transient-photocurrent vs. potential curves for pure Fe, upon

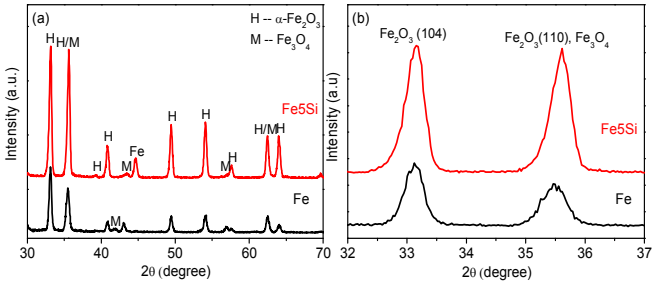

Figure 3. (a) XRD patterns of the oxide films resulting from Fe and Fe5Si alloy annealed at 500 °C for 0.5 h in air + 600 °C for 1 h in Ar and (b) high magnifications between 2θ=32 ° and 37 °.

sweeping the potential from 0.5 V_{RHE} to 1.8 V_{RHE}, the onset of water oxidation photocurrent is at 0.8 V_{RHE}, and the photocurrent increases to 0.4 mA cm^{-2} at 1.23 V_{RHE}. (A higher photocurrent is obtained for nanorod α-Fe_2O_3 than for the air annealing NFs sample (SI, Figure S5a)). For the Fe5Si alloy, most remarkably a significant cathodic shift of onset potential up to 0.4 V_{RHE} can be observed. This value is very close to the flat-band potential of α-Fe_2O_3 (0.4 V_{RHE}) and among the most negative values ever reported.[9]

It is noteworthy that for the Fe-Si alloy not only the suboxide layer thickness is varied; X-ray diffraction (XRD) results (Figures 3 and S6) show stronger hematite peaks for the Fe-Si samples compared to the pure Fe, which indicates a higher crystallinity of the iron oxide structures for the Si containing substrates. This may be in line with reports on minor Si concentrations that affect the crystallinity of Fe_2O_3.[1f] The stronger (104) peak indicates that the c axis of the hexagonal hematite unit cell is aligned perpendicular to the substrate or the basal planes are aligned perpendicular to the substrate. Supported by both the TEM analysis and the dark current onset potentials, and in line with literature[1f], the SiO_2 layer can act as an amorphous buffer that reduces the interfacial strain between the Fe substrate and Fe_3O_4/Fe_2O_3 layers. The reduced interfacial strain would directly lead to better Fe_3O_4/Fe_2O_3 film organization at an atomic level, and is seen directly affect crystallinity (SI, Figure S7). Moreover, the better crystallinity could reduce the boundary defects, which also may explain the improvement of the photocurrent onset potential.

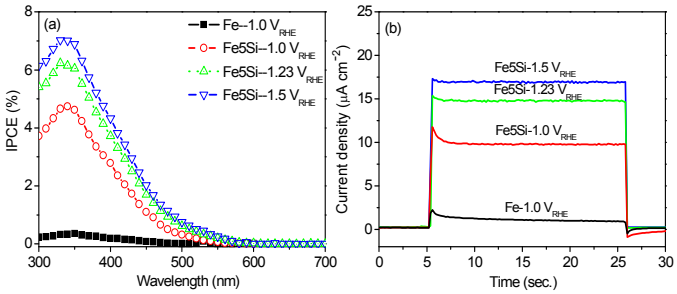

Figure 4. (a) The incident photon conversion efficiency (IPCE) and (b) photocurrent at 360 nm at applied potentials (1.0 V_{RHE}, 1.23 V_{RHE}, and 1.5 V_{RHE}) in 1 M KOH solution of Fe5Si alloy annealed at 500 °C for 0.5 h in air + 600 °C for 1 h in Ar.

Figures 4a shows the incident photocurrent conversion efficiencies (IPCEs) as a function of incident light wavelength for Fe5Si alloy measured at various applied potentials. It is clear that the Fe5Si alloy leads to a significantly enhanced IPCE compared with pure Fe over the entire range from 300 nm to 550 nm. A beneficial effect of the Ar annealing can also be evaluated from the transient photoresponse (Figures 4b). From the figures one can see that the transient ratio values ($i_{steady}/i_{initial}$) close to one have been obtained compared to those in air annealing in the range of 0.02~0.86 (SI, Figure S8). In general, the photo transient reflects strongly on the density and energy of the trapping states.[2a,10,11] In light of XRD results, this can be attributed to the increased crystalline order within the nanorod structure after Ar annealing.

In order to rule out that doping effects of the remaining Si in the Fe_2O_3 structure are the source of the shift in the onset potential, one may consider the following: according to earlier work[12], at least 1at.% Si needs to be present to clearly show a beneficial doping effect in hematite. However, if ToF-SIMS results (SI, Figure S9) are quantified, only a Si concentration < 0.2 at.% in the oxide layer is at maximum present. Therefore, the results presented here strongly suggest the beneficial effect to be due to the impact of crystallography of the iron oxide films and the strongly reduced $Fe_{1-x}O$ layer for the Fe5Si alloy.

Conclusions

In summary, in this work we grow oxide nanostructures by conventional thermal oxidation of Fe and FeSi alloys. A clearly improved water splitting performance is obtained for the Si containing alloy. Particularly, a remarkable cathodic shift of onset potential up to 0.6 V_{RHE} is observed for the Fe5Si alloy. This is one of the most negative onset potentials reported for hematite photoanode devices and is achieved without the use of other catalysts. We ascribe this strong beneficial effect to an accumulation of SiO_2 at the metal/oxide interface – this Si-enriched layer hampers the formation of suboxides, namely Fe_3O_4, which is particularly detrimental for the performance of a hematite based water splitting anode and an increased crystallinity of the Fe_2O_3 layer for layers formed on the Fe-Si alloy.

Acknowledgements

We would like to acknowledge Dr. Natalie Kömpel (Neue Materialien Fürch GmbH, NMF) for GDOES measurements. We thank DFG and the DFG cluster of excellence "Engineering of Advanced Materials" (EAM) for the financial support.

Notes and references

[a] Department of Materials Science and Engineering, WW4-LKO, University of Erlangen-Nuremberg, Martensstr. 7, D-91058 Erlangen, Germany.
Corresponding Author: schmuki@ww.uni-erlangen.de (P. Schmuki)
[b] Department of Materials Science and Engineering, Center for Nanoanalysis and Electron Microscopy (CENEM), University of Erlangen-Nuremberg, Cauerstrasse 6, D-91058 Erlangen, Germany.
[c] Department of Chemistry, King Abdulaziz University, Jeddah, Saudi Arabia.

Electronic Supplementary Information (ESI) available: [details of any supplementary information available should be included here]. See DOI: 10.1039/c000000x/

1 (a) A. Duret and M. Grätzel, *J. Phys. Chem. B* 2005, **109**, 17184. (b) J. Brillet, M. Grätzel and K. Sivula, *Nano lett.* 2010, **10**, 4155. (c) K. Sivula, F. L. Formal and M. Grätzel, *ChemSusChem* 2011, **4**, 432. (d) K. Sivula, R. Zboril, F. L. Formal, R. Robert, A. Weiden kaff, J. Tucek, J. Frydrych and M. Grätzel, *J. Am. Chem. Soc.* 2010, **132**, 7436. (e) S. D. Tilley, M. Cornuz, K. Sivula and M. Grätzel, *Angew. Chem. Int. Ed.*

2010, **49**, 6405. (f) F. Le. Formal, M. Grätzel and K. Sivula, *Adv. Funct. Mater.* 2010, **20**, 1099. (g) L. Wang, C.-Y. Lee and P. Schmuki, *J. Mater. Chem. A* 2013, **1**, 212. (h) L. Wang, A. Palacios-Padrós, R. Kirchgeorg, A. Tighineanu and P. Schmuki, *ChemSusChem* 2014, **7**, 421.

2 (a) M. Frites and S. U. M. Khan, *ECS Trans.* 2009, **19**, 137. (b) H. G. Kim, P. H. Borse, J. S. Jang, C. W. Ahn, E. D. Jeong and J. S. Lee, *Adv. Mater.* 2011, **23**, 2088. (c) C.-Y. Lee, L. Wang, Y. Kado, M. S. Killian and P. Schmuki, *ChemSusChem* in press.

3 (a) M. P. Dareedwards, J. B. Goodenough, A. Hamnett and P. R. Trevellick, *J. Chem. Soc. Faraday Trans.* 1983, **79**, 2027. (b) J. B. Goodenough, *Prog. Solid State Chem.* 1971, **5**, 145. (c) J. H. Kennedy and J. K. W. Frese, *J. Electrochem. Soc.* 1978, **125,** 709.

4 (a) P. Hiralal, S. Saremi-Yarahmadi, B. C. Bayer, H. Wang, S. Hofmann, K. G. Upul Wijayantha and G. A. Amaratunga, *J. Sol. Energy Mater. Sol. Cells* 2011, **95**, 1819. (b) T. Vincent, M. Gross, H. Dotan and A. Rothschild, *Int. J. Hydrogen Energy* 2012, **37**, 8102. (c) L. Wang, C.-Y. Lee, A. Mazare, K. Lee, J. Müller, E. Spiecker and P. Schmuki, *Chem. Eur. J.* 2014, **20**, 77.

5 (a) X. Wen, S. Wang, Y. Ding, Z. L. Wang and S. Yang, J. *Phys. Chem. B* 2005, **109**, 215. (b) A. G. Nasibulin, S. Rackauskas, H. Jiang, Y. Tian, P. R. Mudimela, S. D. Shandakov, L. I. Nasibulina, J. Sainio and E. I. Kauppinen, *Nano Res.* 2009, **2**, 373.

6 (a) Q. Yang, H. Kukino and H. J. Tatsuoka, *Nanosci. Nanotechnol.* 2010, **10**, 7795. (b) X. Su, C. Yu and C. Qiang, *Appl. Surf. Sci.* 2011, **257**, 9014. (c) B. D. Chernomordik, H. B. Russell, U. Cvelbar, J. B. Jasinski, V. Kumar, T. Deutsch and M. K. Sunkara, *Nanotechnol.* 2012, **23**, 194009.

7 (a) N. Beermann, L. Vayssieres, S. E. Lindquist and A. Hagfeldt, *J. Electrochem. Soc.* 2000, **147**, 2456. (b) Z. Chen, U. Cvelbar, M. Mozetic, J. He and M. K. Sunkara, *Chem. Mater.* 2008, **20**, 3224. (c) U. Bjorksten, J. Moser and M. Grätzel, *Chem. Mater.* 1994, **6**, 858.

8 (a) I. Svedung and N. G. Vannerberg, *Corros. Sci.* 1974, **14**, 391. (b) T. Adachi and G. H. Meier, *Oxid. Met.* 1987, **27**, 347. (c) J. Kucera and M. Hajduga, High temperature and long time oxidation of iron and steels, Wydawnictwo PL Filia W Bielsku-Bialej, 1998, **15**. (d) T. Ban, K. Bohnenkamp and H. J. Engell, *Corros. Sci.* 1979, **19**, 291. (e) A. R. Lashin, O. Schneeweiss and Y. Houbaert, *Corros. Sci.* 2008, **50**, 2580.

9 M. T. Mayer, C. Du and D. Wang, *J. Am. Chem. Soc.* 2012, **134**, 12406.

10 (a) N. Birks, G. H. Meier and F. S. Pettit, Introduction to the high temperature oxidation of metals, Cambridge University Press, Cambridge, New York, 2nd edn 2006. (b) M. A. Lukowski and S. Jin, *J. Phys. Chem. C* 2011, **115**, 12388.

11 P. Iwanski, J. Curran, W. Gissler and R. Memming, *J. Electrochem. Soc.* 1981, **128**, 2128.

12 (a) J. H. Kennedy, M. Anderman and R. Shinar, *J. Electrochem. Soc*. 1981, **128**, 2371. (b) J. H. Kennedy, R. Shinar and J. P. Ziegler, *J. Electrochem. Soc*. 1981, **127**, 2307. (c) C.-Y. Lee, L. Wang, Y. Kado, R. Kirchgeorg and P. Schmuki, *Electrochem. Commun*. 2013, **34**, 308.

